

Contents lists available at ScienceDirect

International Journal of Disaster Risk Reduction

journal homepage: www.elsevier.com/locate/ijdrr



Comparison of national and local building inventories for damage and loss modeling of seismic and tsunami hazards: From parcel-to city-scale



Dylan Sanderson*, Daniel Cox

School of Civil and Construction Engineering, Kearney Hall, 1491 SW Campus Way, Oregon State University, Corvallis, OR, United States

ARTICLE INFO

Keywords:
Multi-hazard
Seismic
Tsunami
National structure inventory
Uncertainty
Damage

ABSTRACT

In this paper, we compare the National Structure Inventory, a recently released building inventory for the United States, with a local tax assessor building inventory for use in damage and loss modeling of seismic-tsunami hazards. The city of Seaside, Oregon located in the North American Pacific Northwest and subject to seismic-tsunami hazards from the Cascadia Subduction Zone is used as a testbed. Input attributes - such as spatial footprint, year built, structure type, and number of stories - are compared at the parcel, block, block group, and tract levels. The input attributes show large differences at the parcel level and compare favorably when aggregated at increased spatial scales. The National Structure Inventory consistently underestimates structure value and number of stories compared to the tax assessor data. Expected damages across 7 mean recurrence intervals, from 100-yr to 10,000-yr, are computed using IN-CORE, an open-source community resilience model. Expected damage to the National Structure Inventory tends to be slightly larger than that of the tax assessor data and errors are reduced when aggregated at increased spatial scales. The National Structure Inventory underpredicts total economic losses and risks compared to the tax assessor data, particularly for recurrence intervals associated with high economic risks. A variance-based sensitivity analysis is performed to identify how uncertainties in the input attributes propagate to uncertainties in expected damage. Structure type, designlevel, and building location all influence expected damages for seismic-tsunami hazards, highlighting the importance of accurate building inventories in multi-hazard damage and loss model-

1. Introduction

Modeling and simulation are commonly used in disaster research to improve understanding of disasters, integrate knowledge across disciplines, and provide support in the decision-making process [1–3]. Capturing system-level dynamics, simulation of disasters can incorporate many interacting disciplines – such as urban planning, social sciences, and engineering (e.g., Refs. [4–13]). Damage and loss modeling, a component of disaster simulation, focuses on the impact that natural hazards have on infrastructure systems (e.g., Refs. [14–17,82]). There have been a proliferation of damage and loss models in recent years ranging from loss estimation models [18–20] to more recent state-of-the-art resilience models that consider damage and losses at the parcel-scale, multiple infrastructure systems, and post-disaster recovery [21–23]. As loss estimates from these models inform disaster risk reduction and resilience-increasing decisions, it is imperative that the input data, methods, and resulting output be as accurate as possible [24].

E-mail addresses: sanderdy@oregonstate.edu (D. Sanderson), Dan.Cox@oregonstate.edu (D. Cox).

^{*} Corresponding author.

Natural hazard damage and loss modeling depends on the characterization of the hazard, the building/infrastructure inventories or exposure datasets, and the damage models that map hazard intensity measures to the built environment. For example, the Global Earthquake Model Foundation developed their global earthquake risk model around repositories of probabilistic seismic hazard models, a global exposure dataset, and a set of fragility and vulnerability functions [25]. Uncertainties in the building inventories and exposure datasets exist, and can include, for example, the number, value, and locations of buildings. It has been shown how seismic losses are sensitive to both spatial resolution and location of building inventories [26,27]. The significance of spatial scale and location of buildings are amplified when considering hazards with nonuniform hazard intensity measures over relatively small regions such as floods and tsunamis [28].

In an era of big data, there is an abundance of potential sources where practitioners and researchers can obtain data to represent cities [29,30]. For example, national and global databases of building inventories and methods to create these databases have been developed for seismic and flood hazards [31–33]. In addition, there are critical infrastructure datasets [34], building footprint layers generated from satellite imagery and machine learning (e.g. Refs. [35,36]), and community-driven efforts such as OpenStreetMap in which volunteers collect data from various sources [37]. National and global data sets have been used in damage and loss modeling to evaluate both hazard risks and risk reduction measures (e.g., Refs. [25,38–42]). These results are often evaluated at aggregate spatial scales to make comparisons across different regions.

Different sources of data are often used for smaller scale, local analyses. These can be directly from cities (e.g. Ref. [43]), provided from tax assessor records (e.g. Ref. [44]), or purchased from companies that specialize in real estate data (e.g., Refs. [45,46]). To alleviate human hours in creating these datasets, machine learning methods are being developed that automatically process street view imagery and prepare building inventories for loss assessments [47–49]. Local datasets are commonly employed in damage, loss, and resilience models that operate at small spatial scales, such as the building or parcel level [50]. Access to high-quality, high-resolution data has been identified as a need amongst the natural hazard engineering field [51].

It can be a time-consuming and costly effort to construct an accurate building inventory and it may prove tempting for one to simply use national or global exposure datasets "as-is" in damage and loss models that operate at the building or parcel level. While some researchers have considered how national and local building inventories compare, these studies have either focused on input attributes (e.g. Ref. [52]), or flood hazards (e.g., Refs. [53,54]). With a new generation of damage and loss models that operate at the parcel, or building level, the development and validation of building inventories in both data-rich and data-scarce environments is of interest for both researchers and practitioners [55].

In this paper, we compare the use of a building inventory developed at the national level with a building inventory developed locally for damage and loss modeling of seismic and tsunami hazards. The former is the public version of the National Structure Inventory (NSI), a recently released building inventory for the United States developed by the US Army Corps of Engineers [80]. The local building inventory is composed primarily from a tax assessor dataset. In particular, there are three research questions that this paper addresses:

- 1. How similar are the national and local building inventories as input to damage and loss models? As attributes of buildings influence the resulting damages and losses, this question quantifies the extent to which the NSI and tax assessor datasets are comparable. This includes both the spatial characteristics of the two datasets, e.g., where each building is located, and the attributes associated with each building, e.g., number of stories, structure type. This research question further seeks to understand how these two datasets compare at increasing spatial scales. For example, are the two datasets similar at the parcel level, and if not, what level of spatial aggregation, if any, results in comparable statistics between the two?
- 2. How similar is the output from damage and loss models when using the national and local building inventories as input? Given the similarities and differences between the two datasets identified in the first research question, this question quantifies the extent to which output from a damage and loss model is comparable. Expected damage state and economic losses are considered here. Similar to the first research question, results are compared at increasing spatial scales. This question additionally considers seismic and tsunami hazards across seven mean recurrence intervals to understand how damages and losses between the two datasets compare for varying hazard intensities.
- 3. How do uncertainties in the input attributes propagate to uncertainties in the model outputs? This question considers how sensitive the output from a damage and loss model is to each of the input attributes of a building inventory. The aim is to identify which attributes are most influential. Identification of influential attributes can lead to reduced overall model uncertainty and improved damage and loss estimates for seismic and tsunami hazards. In other words, if one were to improve the accuracy of a building inventory for damage and loss modeling of seismic-tsunami hazards, which attributes are most worthwhile to focus on?

To address these research questions, we consider a testbed in the North American Pacific Northwest subject to seismic-tsunami hazards. Section 2 introduces the testbed and two datasets, then describes the damage and loss model; Section 3 presents the results; Section 4 presents a discussion of the results; and finally, Section 5 summarizes the conclusions.

2. Methods

2.1. Seaside, Oregon testbed and building inventories

The city of Seaside, Oregon, a small coastal town located in the North American Pacific Northwest with a population of 7115 [56] is used as a testbed. Seaside, along with many other coastal communities in the Pacific Northwest, is subject to a rupture of the Cascadia Subduction Zone (CSZ), which is expected to result in a megathrust earthquake and subsequent tsunami [57,58]. Given the exposure to both seismic and tsunami hazards, Seaside has been used extensively as a testbed for multi-hazard damage, loss, and resilience

modeling. This includes a probabilistic seismic-tsunami hazard analysis [59], building and infrastructure damage analyses [60–66], life safety risk analysis [67], and evaluating policies under population growth and urban change [11].

2.1.1. Tax assessor data

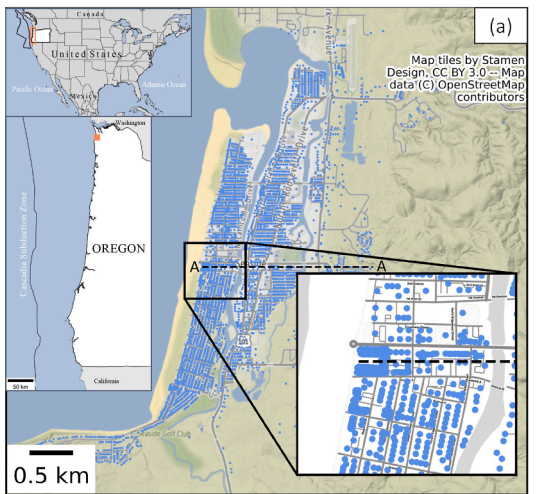
The local building inventory has been used extensively in prior research for the Seaside testbed. The building inventory is primarily composed of tax assessor data from Clatsop County, with Google Street View and a field survey used for spot-checking [60]. Tax assessor data in the United States is commonly collected by local jurisdictions for property tax purposes and there are no nation-wide standards for the type of information collected. Tax assessor data may include information such as property types (e.g., residential, commercial), appraisal value, and square footage. The tax assessor data is from 2012, shown in Fig. 1a, and consists of 4679 buildings [44]. Structure type within the tax assessor data was determined using a "stat class" column and resulted in four specific structure types: light-framed wood structure (W1), commercial and industrial wood (W2), concrete moment frame low-rise (C1L), and concrete moment frame mid-rise (C1M) [60]. The tax assessor data provides an appraisal value that has been adjusted to 2022 USD using an inflation rate of 24% between 2012 and 2022 [68]. Square footage is obtained by mapping Microsoft building footprint data to each point and computing the total area [67,69].

2.1.2. National Structure Inventory (NSI)

The U.S. Army Corps of Engineers (USACE) recently released a public version of the NSI, a nation-wide building inventory for the United States [80]. The NSI contains individual building locations, including attributes, represented as points and has been used by USACE to streamline pre-processing of data to facilitate flood risk modeling. Simultaneously, however, USACE acknowledges that there is sufficient data to consider other hazard types beyond flooding. The NSI data contributes to the Hazus general building stock where it is aggregated at the census block or tract level [70,71]. The NSI data has been used in the past by government agencies or in approved academic work [41,53]. The public version of the NSI provides many useful attributes for damage and loss modeling such as specific occupancy type, square footage, foundation type and height, number of stories, and structure and content values. Some attributes, such as year built, are aggregated at the block level in the public version of the data set to preserve privacy. The NSI data for the testbed is shown in Fig. 1b and consists of 4651 buildings. Although the 2022 NSI data has less buildings than the 2012 tax assessor inventory, a 0.6% difference, we attribute this to the two different sources of data, rather than a decrease in the actual number of buildings in Seaside.

For damage modeling, specific structure types are necessary, whereas only general building types are provided in the NSI data. For example, a general building type may be classified as concrete, while a specific structure type may be concrete moment frame (C1), concrete shear walls (C2), or concrete frame with unreinforced masonry walls (C3). While no specific structure types are provided, the NSI does however provide specific *occupancy types* for each building and the Hazus Inventory Technical Manual has mappings from specific occupancy types, number of stories, and year built to specific structure types [70]. Occupancy type, height, building material, lateral resisting system, and code-level have been used in other studies to inform building damage modeling [72].

Fig. 2 shows a flowchart of how the NSI attributes specific occupancy type, number of stories, and year built are used to define each building's specific structure type and design level. The NSI data has these attributes for each building in Seaside. The "Occupancy Type to Specific Structure Type Database" in Fig. 2 corresponds to the Hazus 4.2 Technical Inventory Manual Tables A-2 to A-10 [70]. These nine tables provide distributions of the specific structure types for US west coast buildings and are dependent on occupancy type, number of stories (low-, mid-, high-rise), and year built. For example, based on occupancy type, number of stories, and year built, a building may have probabilities of 0.2, 0.65, and 0.15 for W1, W2, and C1 respectively. This distribution of structure types could be sampled from, and multiple iterations of building damage computed. This is represented with the "Sample Structure



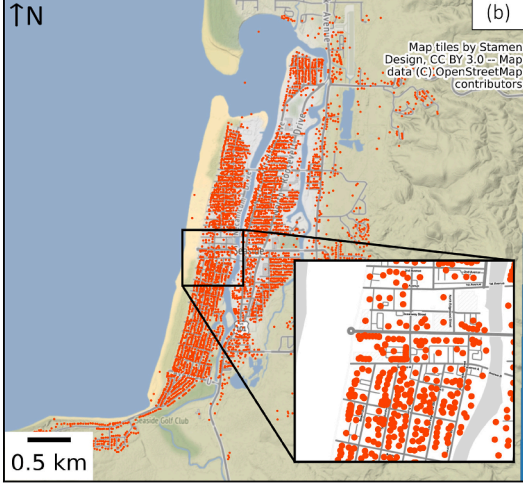


Fig. 1. Location of Seaside, Oregon testbed in the North American Pacific Northwest; shown are (a) 2012 tax assessor data, and (b) 2022 NSI data; buildings are sampled along transect line AA in panel (a) for the sensitivity analysis to address the third research question.

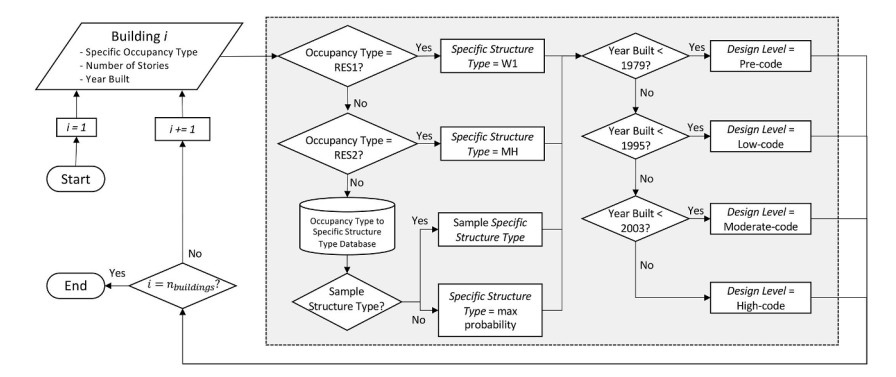


Fig. 2. Flowchart showing assignment of specific structure type and design level from specific occupancy type, year built, and number of stories for buildings in the NSI dataset; specific structure types and design levels are required for the damage modeling.

Type" decision in Fig. 2. Alternatively, the structure type could be assigned as that with the highest probability of occurring – e.g., 0.65 for W2 results in the assignment of W2 structure type. This is the approach taken here. Design-level is additionally required for the damage modeling and correspond to seismic code levels. The design-levels are classified as pre-, low-, moderate-, or high-code. The year-built to design-level mapping is taken from Ref. [60].

2.2. Damage and loss modeling using IN-CORE

Damages and losses for both building inventories are computed using the community resilience model IN-CORE and its python package *pyIncore* [15,22,64,65,66,73,81]. IN-CORE is an open-source community resilience modeling environment used to simulate both the immediate impacts that natural hazards have on the built environment, and subsequent effects such as social and economic losses and post-disaster recovery. Building damage and economic loss modules in pyIncore are used for this study. The building damage model overlays hazard layers on the building inventory and extracts hazard intensity measures at each building. Depending on hazard type, IN-CORE can either generate hazards or use externally generated hazard layers. The latter is used here, and hazard layers are from a probabilistic seismic-tsunami hazard analysis (Fig. 12 of Ref. [59]). These consist of spatially varying hazard intensity measures for seven recurrence intervals. The range of recurrence intervals are used to compare the output from small-to large-magnitude events.

Damage to buildings are computed using the extracted hazard intensity measures at each building and fragility curves to determine the probability being in or exceeding one of four damage states [74]. Hazus fragility curves for both earthquake and tsunami damage are used, and the cumulative damage is computed. The cumulative damage calculations assume that the earthquake and tsunami damage states are statistically independent, except in computing the probability of complete and extensive damage [75,76]. Additional details about using IN-CORE for seismic-tsunami damage and computing the cumulative damage can be found in Refs. [61,62,65]. To determine a single value for building damage, the expected damage state, *E[DS]*, is computed as:

$$E[DS] = \sum_{i=0}^{3} i \cdot P(DS_i)$$
 (1)

where $P(DS_i)$ is the probability that the building is in damage state i, which can take on values of 0 (none/insignificant damage), 1 (moderate damage), 2 (extensive damage), or 3 (complete damage). Taking the expectation of the damage state results in a continuous value between 0 and 3.

Economic losses in IN-CORE are computed using methods from Ref. [20]. The mean damage is first computed by multiplying the probability of being in each damage state with damage ratios and taking the sum. The economic losses are then computed by multiplying the mean damage by each building's value. Economic losses for the NSI data use the provided structure value, whereas economic losses for the tax assessor data use the appraisal value adjusted to 2022 USD with an inflation rate of 24% [68]. In computing the cumulative losses, the cumulative probability of being in each damage state is used. Economic risks are defined as the losses multiplied by the annual exceedance probability, or inverse of the mean recurrence interval [77]. Economic risks help identify recurrence intervals and hazards that result in both large economic losses and have a higher probability of occurrence [65].

3. Results

3.1. Comparison of datasets as input to damage and loss models

The spatial location and attributes of the NSI and tax assessor datasets are first compared prior to running IN-CORE. Four spatial scales – parcel, block, block group, and tract – are considered to visualize differences in the spatial footprints of the two datasets. Parcels are the smallest scale considered here and are typically used for tax purposes to delineate properties. According to the US Census Bureau, blocks are statistical areas bounded by features such as streets, streams, and railroad tracks, block groups are clusters of blocks that contain between 600 and 3000 people, and census tracts are subdivisions of a county that typically contain 1200 and 8000 people [78]. The percent difference within a single polygon is computed and normalized by the average number of points in that poly-

gon. For example, if a single parcel contains 3 NSI points, and 2 tax assessor points, the percent difference is computed as +40%, the difference of 3 NSI points and 2 tax assessor points divided by 2.5 – the average of 3 and 2. Fig. 3 shows the percent difference in number of points in each parcel (3a), block (3 b), block group (3c), and tract (3d). Red polygons indicate that there are more NSI points than tax assessor points in that polygon, whereas blue polygons indicate the reverse. Grey polygons indicate that there are the same, number of NSI and tax assessor points in that particular polygon. Fig. 3a shows that at the parcel-level there are a considerable number of polygons that have both the same number of NSI and tax assessor points and those that differ. At the block group level (3c), the shoreward most block group compares favorably, whereas to the east there are more NSI points than tax assessor points. Fig. 3d shows that when aggregating to the census tract-level, the percent difference between the number of points in each tract approaches 0%.

To quantify the differences in the NSI and tax assessor data, Fig. 4 shows relationship plots at the four aggregating spatial scales. The dashed line in each plot shows perfect agreement. Pearson correlation coefficient, slope from a regression analysis, and normalized root mean square error (NRMSE) are computed and shown in the lower right corner of each plot in Fig. 4. The Pearson correlation coefficient ranges between -1 and 1. The slope is computed using an orthogonal distance regression with the intercept set to 0. The NRMSE is normalized by the average; here, that is the average number of points in all polygons for that aggregating scale. Fig. 4 shows how as the spatial scale that the points are aggregated at increases, differences in the number of points within each polygon become smaller. At the parcel-level (4a), the points are not highly correlated ($\rho = 0.448$) and have an NRMSE value of 1.408. As the aggregating spatial scale increases from parcel to tract, the correlation coefficients increase such that at the this becomes 0.999 at the tract-level and the NRMSE is 0.038.

Building attributes of structure value, year built, square footage, and number of stories are also compared. These attributes are aggregated and averaged at each of the four spatial scales. For instance, considering the example above with 3 NSI points and 2 tax assessor points in a single polygon, the average number of stories of the 3 NSI points are compared with the average number of stories for the 2 tax assessor points. This process is repeated for all polygons. In computing the NRMSE, each data point is weighted according to the number of points within the aggregating polygon, and the NRMSE is normalized by the average of the observations. In the example above, the 3 NSI points and 2 tax assessor points would be assigned a weight of 5. In computing the NRMSE, the weights are considered for attributes that are aggregated and averaged. No weight is considered when comparing the number of points in each polygon to avoid double counting.

Fig. 5 shows how these attributes compare across the four spatial scales – parcel, block, block group, and tract. Each row of Fig. 5 correspond to the same statistics (correlation coefficient, slope, and NRMSE) shown in Fig. 4, with the first column of Fig. 5 corresponding to the results shown in Fig. 4. The correlation coefficient approaches 1 for number of points, year built, and num-

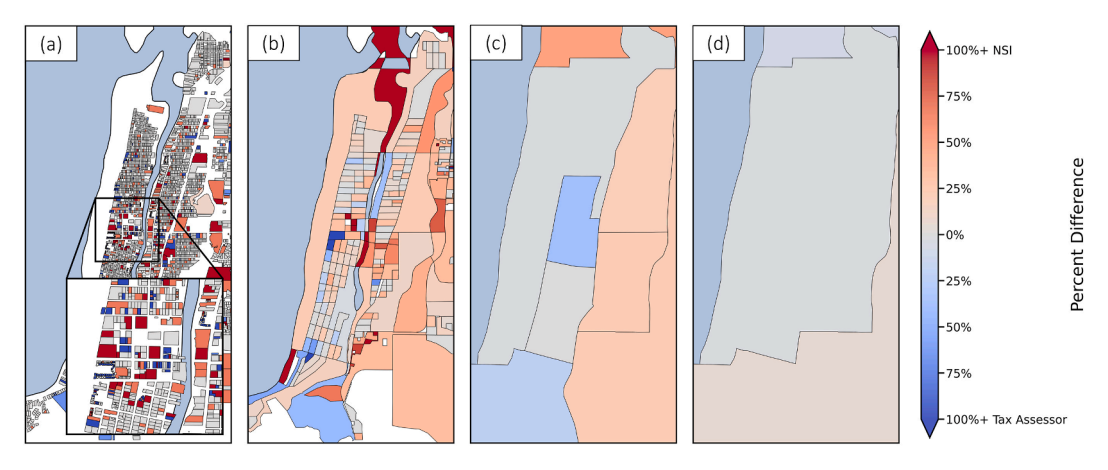


Fig. 3. Percent difference in number of points in each: (a) parcel, (b) block, (c) block group, and (d) tract; red polygons indicate more NSI points than tax assessor, blue indicates the opposite.

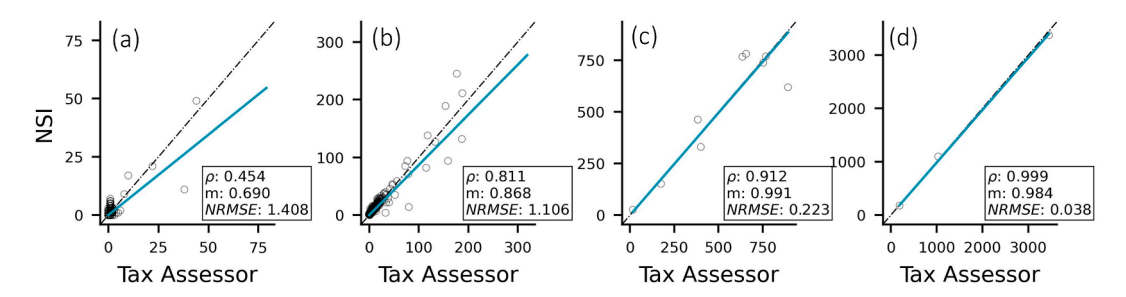


Fig. 4. Relationship plots showing number of points in each: (a) parcel, (b) block, (c) block group, and (d) tract; correlation coefficient (ρ), slope from regression (m), and normalized root mean square error (NRMSE) are shown in the lower right corner of each plot.

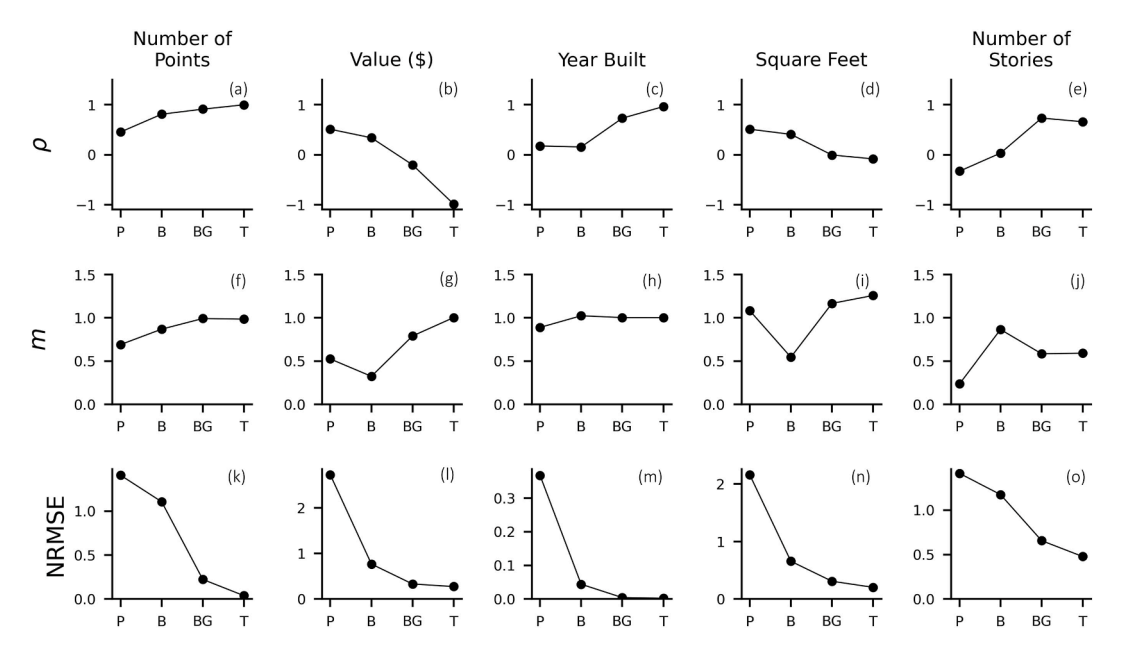


Fig. 5. Correlation coefficient (ρ), slope (m), and normalized root mean square error (NRMSE) (rows) from relationship plots for number of points, structure value, year built, square feet, and number of stories (columns); points are aggregated at the parcel (P), block (B), block group (BG), and tract (T) levels.

ber of stories as the spatial scale increases. Fig. 5g and j both show that the NSI data consistently underestimates the structure value and number of stories at the parcel-level as the slope is less than 1.

The NRMSE decreases as the aggregating spatial scale increases. The decrease in NRMSE from block group to tract tends to be less pronounced indicating that the NSI and tax assessor datasets tend to compare favorably at the block group level for all attributes. For some attributes, such as structure value, year built, and square feet, the datasets compare favorably at the block level.

The structure value and square footage both have decreasing correlation coefficients while also resulting in decreasing NRMSE as the aggregating spatial scale is increased. For structure value, the small NRMSE at the block group and tract levels (Fig. 51) is due to the relatively small differences between the two datasets, considering that this statistic is normalized by the average of structure values in all block groups and tracts respectively. On the other hand, the structure value correlation coefficient at the tract level is -0.989, indicating that the points associated with this statistic are aligned along a straight line that slopes downward. (It should be noted that this is not reflected in the slope calculations as the regression analysis has an intercept set to 0, thus resulting in positive slopes.) Another way to visualize this is that if there were two sets of points, both of which have a correlation coefficient near to -1, the location of these sets of points along the line could be either tightly grouped (resulting in a low NRMSE) or significantly spread out (resulting in a large NRMSE). This same logic applies to the square footage correlation coefficient and NRMSE calculations, except in this case, the correlation coefficient is near 0. Here, the points are tightly grouped, but do not have a strong linear relationship.

Specific structure types of both the NSI and tax assessor data are compared at the parcel-level only for parcels that have a one-to-one mapping. That is, only parcels that have one NSI point and one tax assessor point are considered here. This resulted in 3037 points out of the original 4679 tax assessor and 4651 NSI buildings, an approximately 65% retention. Fig. 6 shows a matrix comparing these specific structure types, with descriptions of the structure type abbreviations provided to the right of the matrix. The tax assessor data has four structure types, W1, W2, C1L, and C1M, whereas assigning structure types to the NSI data from the occupancy type results in 9 structure types for the 3037 points. There are 1919 buildings in the NSI and tax assessor datasets that both are classified as W1, light-frame wood structures. The majority of buildings in Seaside are wood-framed, single-family homes, hence the strong correlation for W1 structures between the NSI and tax assessor datasets. The assignment of structure types for the NSI data resulted in no C1L and C1M structures, whereas concrete structures in the tax assessor data are assigned to these specific structure types. Instead, the NSI data has C2L and C2M structures. This is because it is often difficult to distinguish specific structural attributes of individual buildings.

Of these 3037 points that have a one-to-one mapping, 1920 (63.2%) have the same structure type, 1757 (57.9%) have the same design level, and 2138 (70.4%) have the same number of stories. Considering two attributes simultaneously: 1272 buildings (41.9%) have the same structure type *and* design-level, 1556 (51.2%) have the same structure type *and* number of stories, and 1245 (41.0%) have the same design-level *and* number of stories. Finally, considering all three attributes, 988 out of the 3037 buildings (32.5%) have the same structure type, design-level, and number of stories.

3.2. Comparison of damages and economic losses

Fig. 7 shows the expected damage states of both the NSI and tax assessor buildings for the 500-yr recurrence interval seismictsunami hazard. As expected, buildings near to the shoreline see more damage as they are subject to tsunami inundation. There are a few NSI buildings in Fig. 7a that are located inland and are completely damaged. These buildings are classified as mobile homes when

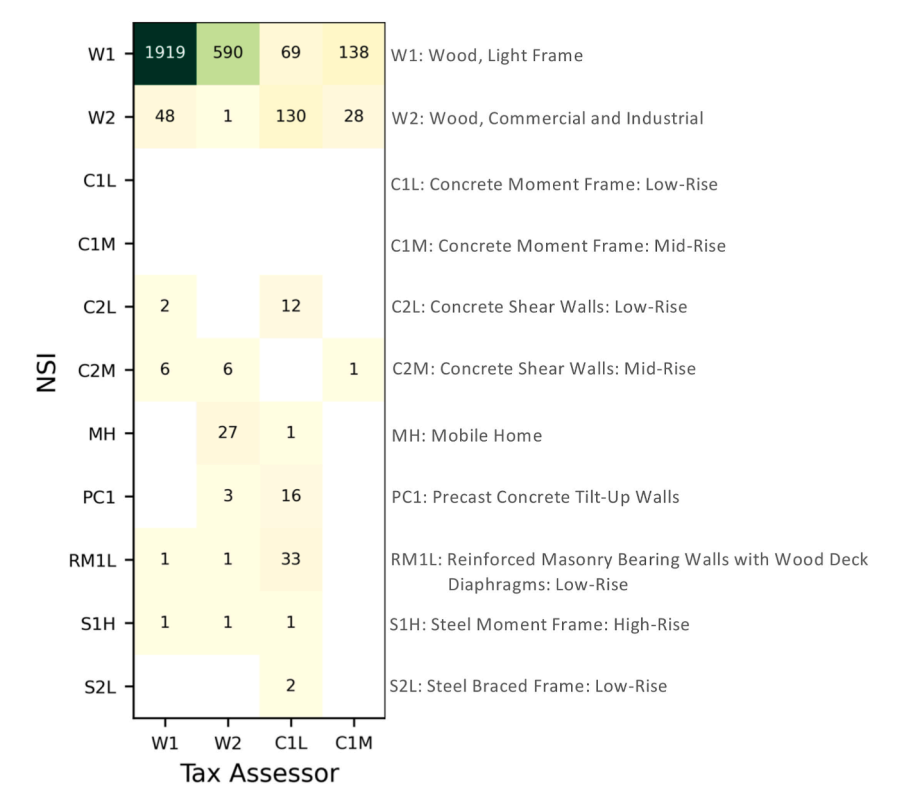


Fig. 6. Matrix counting structure type assignments for 3037 points that have a one-to-one matching at parcel-level.

assigning specific structure types, and the fragility curves for these are particularly vulnerable to tsunami hazards. The insets maps Fig. 7b and e shows differences in the expected damage when comparing building-to-building. The cluster of completely damaged NSI buildings in the red circle are classified as light-framed wood, W1, structures, whereas their tax assessor counterparts are assigned as concrete moment frame structures, C1L and C1M. Inset maps of Fig. 7c and f shows how the expected damage can also compare favorably between the two datasets. The shoreward-most buildings here result in large levels of expected damage, whereas those to the south result in less expected damage. This is caused by the extent of tsunami inundation as there are sharp gradients in inundation at this area.

Fig. 8 shows the expected damage state across 7 recurrence intervals from 100-yr to 10,000-yr. The root mean square error (RMSE) is shown in the lower right of each plot. Similar to Figs. 3–5, the expected damages are aggregated at the parcel, block, block group, and tract levels by taking the average of the expected damage state within each aggregating polygon. Each point in Fig. 8 is color-coded according to the distance from the shoreline to the polygon centroid. Fig. 8 shows how polygons closer to the shoreline result in more damage as the buildings within these polygons are subject to both seismic and tsunami hazards. Regardless of the spatial scale, the influence of increasing the recurrence interval from the 100-yr event to the 10,000-yr event can be seen as the points shown in Fig. 8 shift from the lower left corner to the upper right corner. At the parcel-level, the largest error occurs at the 500-yr, 1000-yr, and 2500-yr recurrence intervals. The error decreases for the remaining recurrence intervals as buildings are either slightly damaged or are completely damaged.

As the aggregating spatial scale is increased from parcel to tract, errors in the expected damage decrease. At the parcel-level, the expected damage differs significantly due to differences in structure type, year built, etc.; however, by aggregating the buildings within larger geographic regions, there is not as much variability. This is similarly seen in the previous section comparing input where the NRMSE decreases as the spatial scale increases.

The 100-yr recurrence interval results in a line of best fit greater than 1, particularly at the parcel and block levels. This is due to the occurrence of mobile home structure types (MH) in the NSI dataset whereas the tax assessor dataset does not have any buildings of this type. The fragility curves for these structure types result in high expected damage states. The remaining line of best fits in Fig. 8 show that the NSI tends to slightly overpredict damages compared to the tax assessor data.

Fig. 9 shows economic losses (first row), economic risks (second row), and percent difference between the NSI and tax assessor losses/risks (third row). The economic risk plots, Fig. 9d–f, identify recurrence intervals that result in both large losses *and* have a higher probability of occurring. Positive values in the percent difference indicate that the NSI losses/risks are greater. The total expected losses and risks are deaggregated by hazard type and shown for all 7 recurrence intervals. Fig. 9h shows that the earthquake-only economic losses/risks result in the largest variation for the 500- to 5000-yr recurrence intervals with a percent difference of up to –21.9%. Conversely, recurrence intervals associated with the largest tsunami-only economic risks result in low percent difference

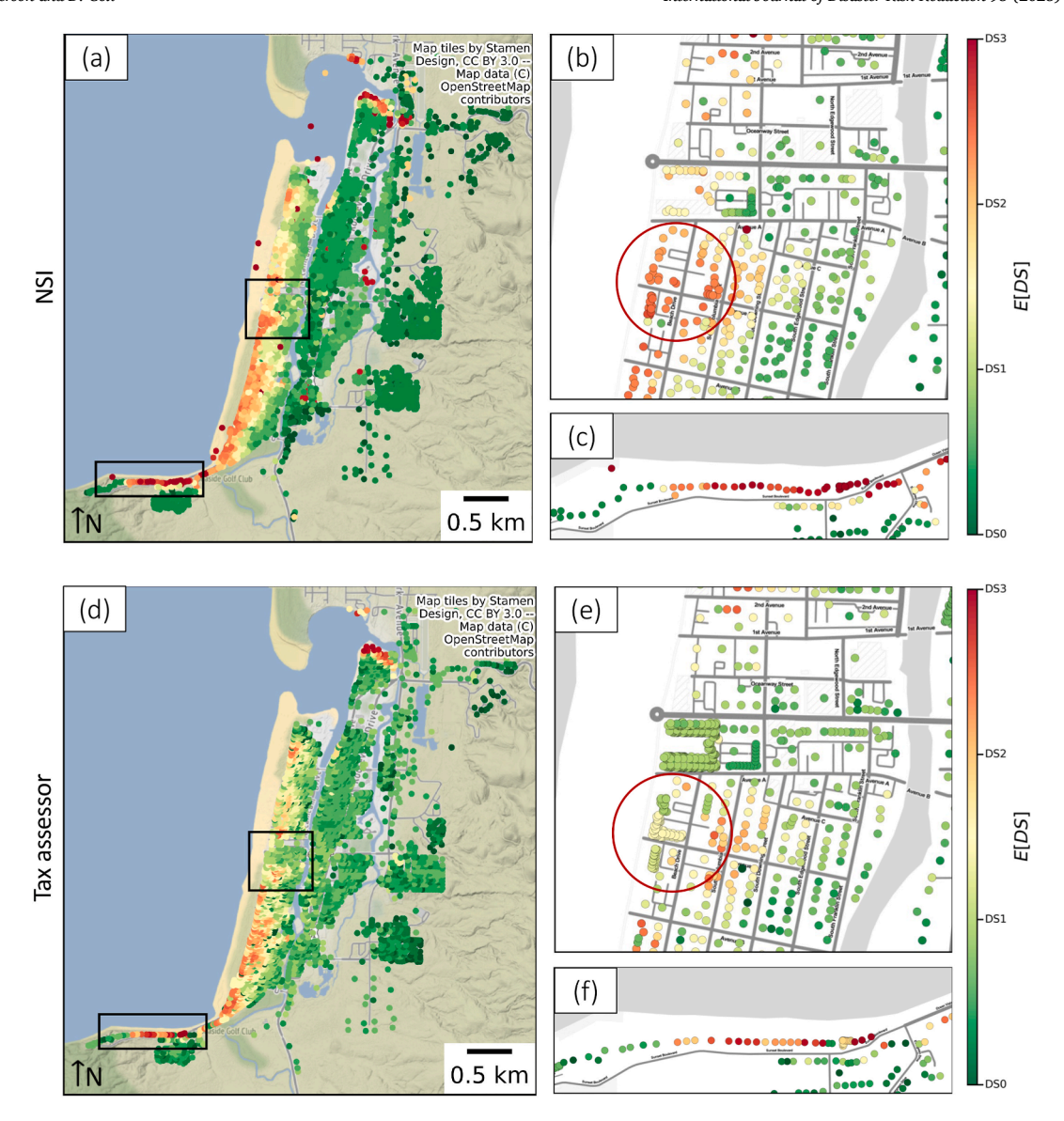


Fig. 7. Expected damage state of NSI (top row; panels a, b, and c) and tax assessor buildings (bottom row; panels d, e, and f) for the 500-yr recurrence interval.

between the NSI and tax assessor data. Fig. 9j shows that the largest percent difference for the cumulative seismic-tsunami losses/risks is -15.1% at the 500-yr recurrence interval. This recurrence interval results in the largest economic risks (Fig. 9f).

Across nearly all recurrence intervals, the NSI data underpredicts economic losses and risks compared to the tax assessor data, while at the same time slightly overpredicts expected damages (Fig. 8). This is due to the structure values in the NSI and tax assessor data. Fig. 5g shows how the slope comparing the structure value is below 1 at the parcel level, indicating that the NSI structure values are consistently below the tax assessor values. These results highlight the importance of both accurate structure values and damage estimates for economic loss/risk calculations.

3.3. Sensitivity analysis identifying most influential input attributes

Variance-based sensitivity methods are used to attribute overall variance in the output to both individual input variables and interactions between input variables [79]. Three input attributes are considered: (1) design-level, (2) structure type, and (3) building location. The design-level and structure type are used to identify fragility curves for computing damage. These attributes are varied over their entire input space. That is, the structure type is varied over each of the 36 Hazus structure types, whereas the design-level is varied across pre-, low-, moderate-, and high-code. Building location, on the other hand, influences the hazard intensity measures a building is subject to. For the sensitivity analysis, the building locations are varied over 100 equally spaced points along the transect line AA shown in Fig. 1a. In all, this resulted in 14,400 independently and uniformly distributed input sample points: 36 structure types \times 4 design-levels \times 100 building locations. The remaining input attributes, such as square-footage and building value, are not

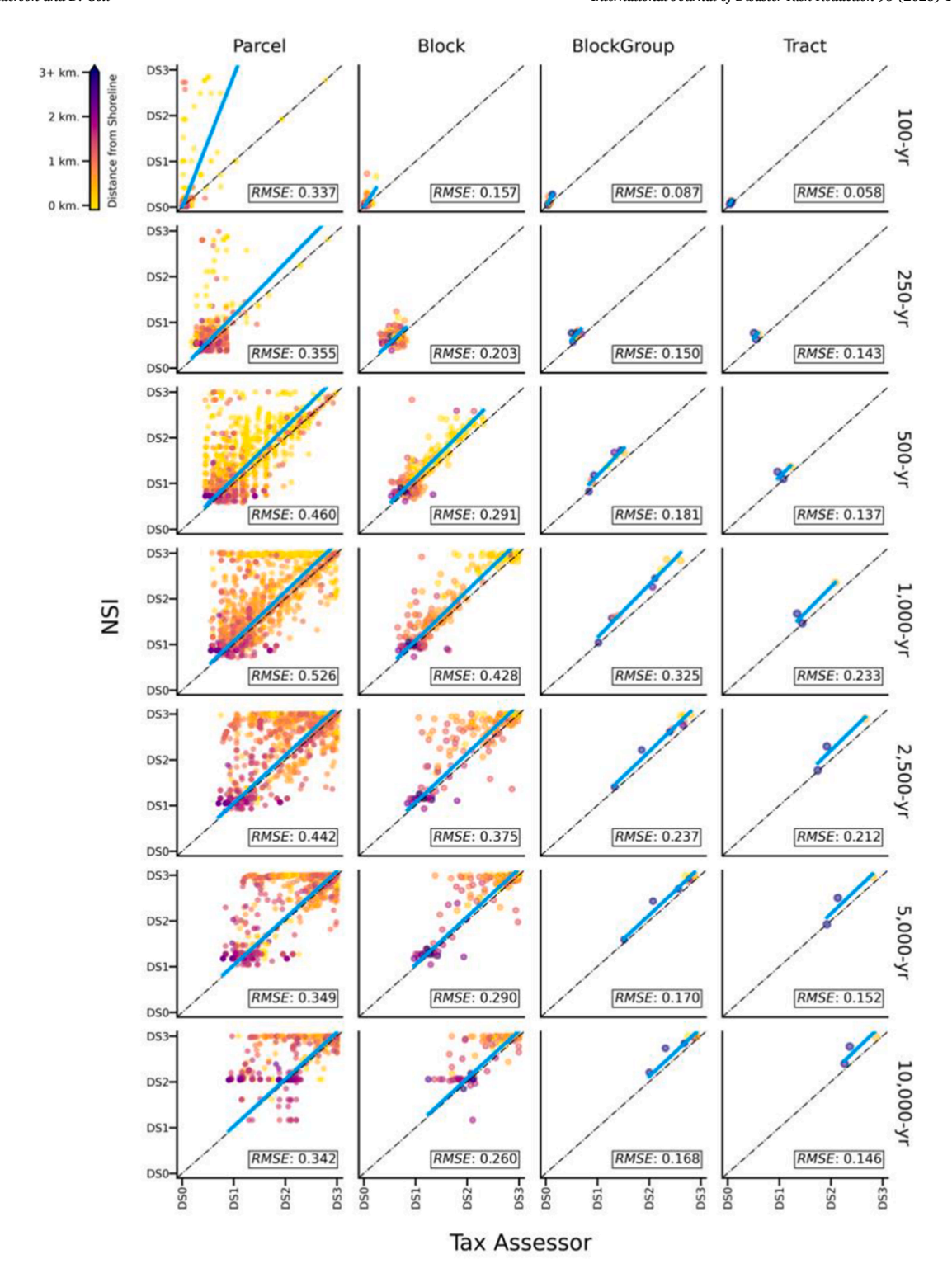


Fig. 8. Average expected damage states from tax assessor (x-axis) and NSI (y-axis) across recurrence intervals (rows) and spatial scales (columns); line of best fit from orthogonal regression is shown in cyan; each point is color-coded by distance from the shoreline.

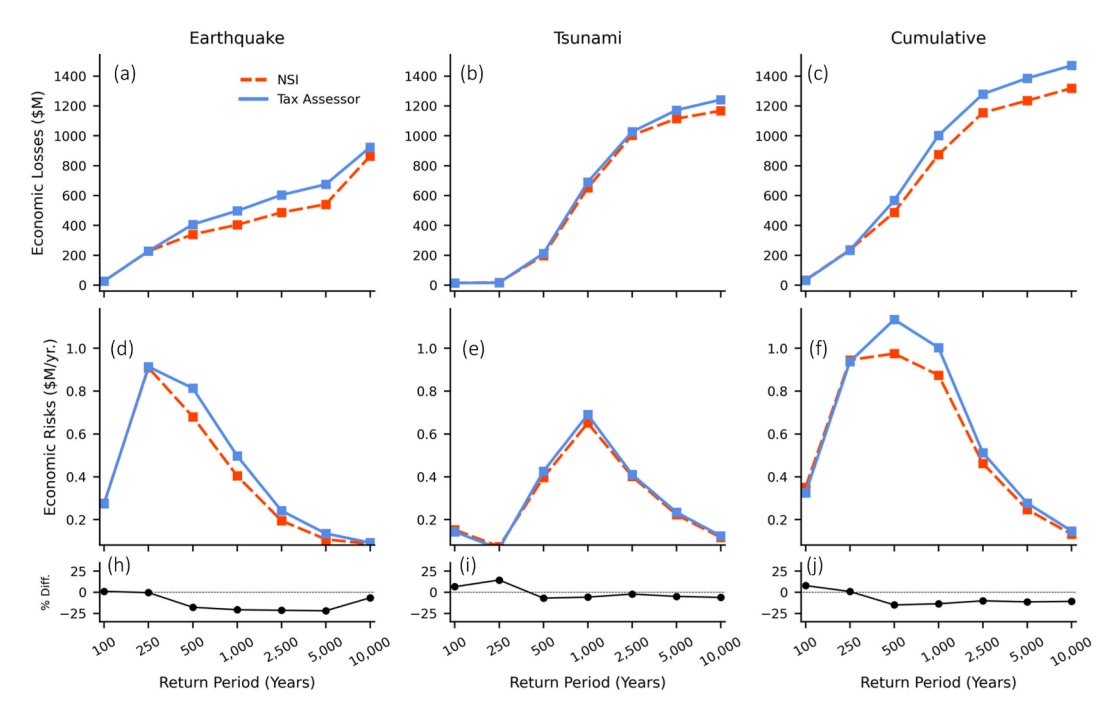


Fig. 9. Direct economic losses (top row) and risks (bottom row) for NSI and tax assessor datasets across recurrence intervals and deaggregated hazards (columns).

considered here as they do not directly influence the building damage. Seismic, tsunami, and cumulative damage across the seven recurrence intervals are computed, and the output considered is the expected damage state as provided in Equation (1). First- and second-order Sobol indices are then computed as:

$$S_i = \frac{V_i}{V(Y)} = \frac{V_{x_i} \left[E_{x_{\sim i}} \left(Y | X_i \right) \right]}{V(Y)} \tag{2}$$

$$S_{ij} = \frac{V_{ij}}{V(Y)} = \frac{V_{x_{ij}} \left[E_{x_{\sim ij}} \left(Y \middle| X_i, X_j \right) \right] - V_i - V_j}{V(Y)}$$
(3)

Where V_i corresponds to the variance in the model output due to variation of input attribute i. Similarly, V_{ij} corresponds to the variance in the model output due to the interaction of attributes i and j. Large values of S_i and S_{ij} indicate that attribute i, or the interaction of attributes i and j, are important.

Fig. 10 shows the first- and second-order Sobol indices for design level (DL), structure type (ST), and building location (BL). First order indices are a darker shade compared to the second order. The Sobol indices are deaggregated by recurrence interval and hazard type. The summation of *SI* in the upper right corner of each subplot indicates how much of the variance is explained by the indices shown. A value of 1.0 indicates that 100% of the variance is explained. For the plots that have a value less than 1.0, the remaining variance is explained by the interaction of all three input attributes.

Fig. 10a–g show that design level and structure type explain nearly all of the variance in the model output for earthquake only damage. This is because the earthquake hazard is nearly uniform over the study area, and the expected damage state is not sensitive to where the building is located. As the recurrence interval increases, the earthquake damage is more sensitive to the structure type rather than the design-level. There is some interaction between structure type and design level for the 100-yr recurrence interval; however, this becomes negligible at higher recurrence intervals. If a practitioner or researchers is only considering earthquake hazards, then having good data on the structure type is beneficial.

The tsunami-only damage indicates that the model is sensitive to the interaction of structure type and building location for small recurrence intervals (Fig. 10h and i). Small recurrence intervals do not result in much tsunami inundation compared to the high recurrence intervals. As such, the model is particularly sensitive to both where the building is located, e.g., in or out of the inundation zone, and what the structure type is, e.g., a mobile home vs. a concrete building. As the recurrence interval increases, the interaction effects between structure type and building location decreases. Simultaneously, more variation is explained by only the building location. This implies that regardless of the structure type of a building, whether that building is in or out of the inundation zone is important.

Considering the cumulative damage resulting from both earthquake and tsunami, Fig. 100 shows that the majority of the variation in damage for the 100-yr recurrence interval is driven by the interaction effects between structure type and building location. At the 250-yr recurrence interval, Fig. 10p, structure type becomes important indicating most of the variation is driven by the earthquake hazard. Considering that the 250-, 500-, and 1000-yr recurrence intervals result in the largest economic risks, Fig. 10p to r show that

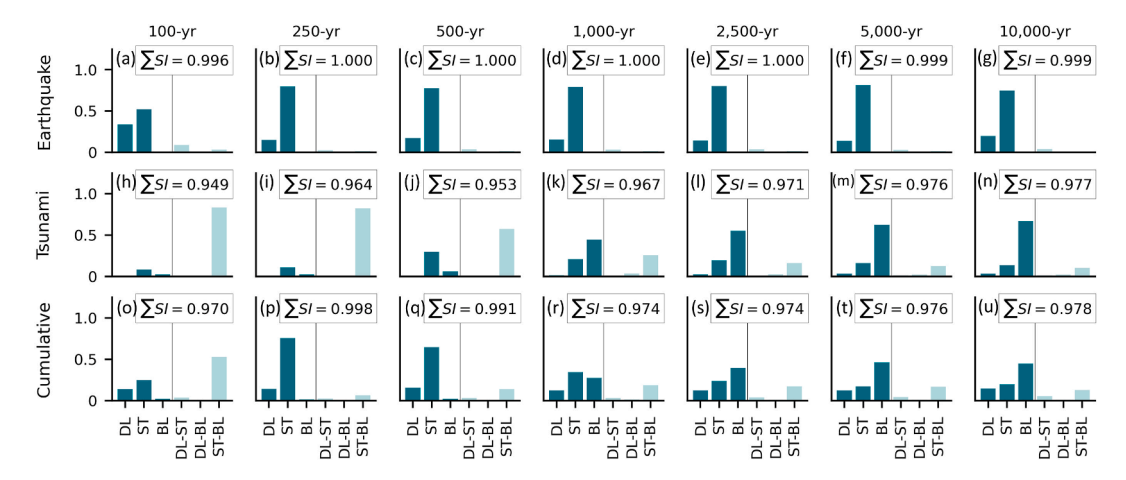


Fig. 10. First and second-order Sobol Indices explaining variation in expected damage state for three input attributes: Design Level (DL), Structure Type (ST), and Building Location (BL); results are deaggregated across hazard type (rows) and recurrence interval (columns); the summation in the top right of each plot indicates the sum of the first and second-order Sobol indices.

the structure type and building location are important. Further, the design-level of the buildings is not to be neglected as it explains a considerable amount of variance in the output. Because no single attribute stands out in explaining most of the variance for the cumulative seismic-tsunami hazard, this highlights the importance of accurate data to be used in damage and loss models.

4. Discussion

As constructing an accurate building inventory for damage and loss modeling can be a time-consuming and costly effort, practitioners and researchers may be interested in using publicly available national and global datasets "as is". Results for the Seaside test-bed highlight that a national-level datasets can compare favorably to a locally constructed tax assessor dataset if aggregating results at increased spatial scales. The largest error between the two datasets occurred at the parcel-level, highlighting the differences at a building-by-building level. As such, if one is interested in damage and loss modeling at the parcel-level, rather than aggregate scales, additional attention should be given to the input. Aggregating the results at increased spatial scales, however, results in decreased errors between the two datasets both as input to- and output from-the damage and loss model. Aggregating and averaging building value, year built, and square footage at the block-level best reduces discrepancies while preserving some spatial heterogeneity. The number of points and number of stories must be aggregated and average at the block group level to achieve similar results. Mostafiz et al. [53] have also found that comparing the NSI to a locally constructed dataset results in building-by-building differences but found no statistically significant difference at aggregate spatial scales.

The economic loss and risk calculations highlight how differences in the two datasets can propagate as additional analyses are chained together. Whereas the damage estimates compared favorably at the tract level across all recurrence intervals (Fig. 8), the total economic losses at the city level had percent differences of up to 20% (Fig. 9). With these large discrepancies, this highlights the need for accurate structure replacement values, and one should be mindful of these large errors. Total economic losses for the NSI data were consistently underestimated compared to the tax assessor data for seismic tsunami hazards. Yildirim et al. [54] have also observed that for flood hazards, national-level datasets can underestimate economic losses compared to locally constructed datasets.

Results from the sensitivity analysis can be used to help practitioners and researchers who consider damages and losses from seismic and/or tsunami hazards. Structure type and design-level play an important role in the sensitivity of the expected damage due to earthquakes, as opposed to building location, because the hazard is uniform for the testbed. With more accurate data regarding these attributes, practitioners can obtain more accurate estimates of expected damage. On the other hand, expected damage resulting from tsunami hazards was shown to be particularly sensitive to the building location because of the strong gradient in hazard intensity, followed by structure type. As the location of a building influences the tsunami hazard intensity measure a building is subject to, this highlights the importance of both accurate estimates of building locations and tsunami inundation modeling. One limitation of the sensitivity analysis is that Hazus seismic and tsunami fragility curves were used to compute expected damage. The results presented here could be particularly sensitive to the damage models employed.

The NSI data was selected in this study as a version of this dataset was recently made publicly available. As more researchers and practitioners may begin to use the NSI data for damage and loss modeling in the United States, it is of interest to understand how this national dataset compares to locally generated datasets both as input to and output from damage and loss models. As additional methods to construct building inventories for damage and loss modeling continue to be developed, such as those using machine learning and computer vision, currently an active area of research, the methods outlined in this manuscript can be used to compare how uncertainties in two or more building inventories propagate to uncertainties in damage and loss outputs. Similarly, the methods outlined herein could be used beyond the United States for comparing two or more building inventories. Further, this study highlights how regional damage and loss models are sensitive to the building inventories that serve as input.

5. Conclusions

National and global datasets of infrastructure systems are increasingly becoming popular for use in damage and loss modeling. These datasets are typically used to compare damages and losses resulting from natural hazards across large geographic regions. Historically, locally constructed datasets, such as those provided directly from cities or tax assessor offices have been used for damage and loss models that operate at the parcel or building level. Given the time and effort needed to construct a building inventory, researchers may be tempted to use national and global datasets "as is" in damage and loss models that operate at the parcel or building level. This paper compared a national and local building inventory for use in damage and loss modeling of seismic and tsunami hazards. The national dataset used here is the public version of the National Structure Inventory (NSI), a recently released building inventory for the United States, whereas the local building inventory is composed primarily from a tax assessor data.

The following conclusions can be obtained for the Seaside testbed:

- 1. The NSI and tax assessor datasets compare favorably when aggregated at the block, block group, and tract level despite large differences at the parcel level. It was shown how differences in the input attributes decrease as the two datasets are aggregated and averaged at increasing spatial scales (Fig. 3, Fig. 4, and Fig. 5). Aggregating and averaging building value, year built, and square footage at the block-level best reduces discrepancies while preserving some spatial heterogeneity. Conversely, the number of points and number of stories must be aggregated and average at the block group level to achieve similar results. The NSI data consistently underestimates the structure value and number of stories compared to the tax assessor data regardless of the aggregating scale that is used for comparison.
- 2. Damages to the NSI and tax assessor data compare favorably when aggregated at increased spatial scales, whereas total economic losses for the city resulted in large differences. It was shown that when expected damages were aggregated at the block, block group and tract levels, the average damages compared favorably (Fig. 8). The total economic loss and risk results, however, did not compare as favorably when aggregated at the city level (Fig. 9). The NSI data underpredicted the total economic losses and risks for nearly all recurrence intervals.
- 3. The expected damage of buildings resulting from seismic-tsunami hazards is sensitive to structure type, design-level, and building location; thus, emphasizing the importance of accurate data in damage and loss modeling. It was shown that damage resulting from earthquake-only hazards is foremost sensitive to the structure type, followed by the design-level. For tsunami-only hazards, the building location plays the most important role, emphasizing the importance of accurate building location and tsunami inundation modeling (Fig. 10). Together these results highlight the importance of accurate building inventories in multi-hazard damage and loss modeling.

Future work could explore how the uncertainties in the input propagate through additional chained analyses such as population dislocation, computable general equilibrium modeling, and post-disaster restoration times. Additional sources of building inventories, including those available for purchase and those generated using machine learning methods could be compared alongside global, national and local datasets.

Declaration of competing interest

The authors declare that they have no known competing financial interests or personal relationships that could have appeared to influence the work reported in this paper.

Data availability

Data will be made available on request.

Acknowledgements

We acknowledge funding in part through Oregon Sea Grant under award no. NA18OAR170072 (CDFA no. 11.417) from NOAA's National Sea Grant College Program, US Department of Commerce, and by appropriations made by the Oregon State Legislature; the cooperative agreement 70NANB15H044 between the National Institute of Standards and Technology (NIST) and Colorado State University through a subaward to Oregon State University; and the National Science Foundation through award NSF-2103713. The content expressed in this paper are the views of the authors and do not necessarily represent the opinions or views of NIST or the U.S Department of Commerce.

References

- [1] R. Davidson, L. Nozick, Computer simulation and optimization, in: H. Rodríguez, W. Donner, J. Trainor (Eds.), Handbook of Disaster Research, second ed., 2018, pp. 331–356, https://doi.org/10.1007/978-3-319-63254-4 17.
- [2] A. Reilly, R. Dillon, S. Guikema, Agent-based models as an integrating boundary object for interdisciplinary research, Risk Anal. 41 (7) (2018), https://doi.org/10.1111/risa.13134.
- [3] A. Mostafavi, N. Ganapati, Toward convergence disaster research: building integrative theories using simulation, Risk Anal. 41 (7) (2021), https://doi.org/10.1111/risa.13303.
- [4] National Institute of Standards and Technology (NIST), Community Resilience Planning Guide for Buildings and Infrastructure Systems, vol. 1, National Institute of Standards and Technology, Washington, D.C, 2016, https://doi.org/10.6028/NIST.SP.1190v1.
- [5] D. Wang, R. Davidson, L. Nozick, J. Trainor, J. Kruse, Computational framework to support government policy-making for hurricane risk management, ASCE Natural Hazards Review 21 (1) (2020), https://doi.org/10.1061/(ASCE)NH.1527-6996.0000348.
- [6] C. Galasso, J. McCloskey, M. Pelling, M. Hope, C. Bean, G. Cremen, R. Guragain, U. Hancilar, J. Menoscal, K. Mwang'a, J. Phillips, D. Rush, H. Sinclair, Risk-

- based, pro-poor urban design and planning for tomorrow's cities, Int. J. Disaster Risk Reduc. 58 (2021), https://doi.org/10.1016/j.ijdrr.2021.102158.
- [7] M. Hemmati, H. Mahmoud, B. Ellingwood, A. Crooks, Shaping urbanization to achieve communities resilient to floods, Environ. Res. Lett. 16 (2021), https://doi.org/10.1088/1748-9326/ac1e3c.
- [8] M. Hemmati, H. Mahmoud, B. Ellingwood, A. Crooks, Unraveling the complexity of human behavior and urbanization on community vulnerability to floods, Nature Scientific Reports 11 (1) (2021) 1–15, https://doi.org/10.1038/s41598-021-99587-0.
- [9] G. Cremen, C. Galasso, J. McCloskey, A simulation-based framework for earthquake risk-informed and people-centered decision making on future urban planning, Earth's Future 10 (1) (2022), https://doi.org/10.1029/2021ef002388.
- [10] C. Guo, L. Nozick, J. Kruse, M. Millea, R. Davidson, J. Trainor, Dynamic modeling of public and private decision-making for hurricane risk management including insurance, acquisition, and mitigation policy, Risk Manag. Insur. Rev. 25 (2022) 173–199, https://doi.org/10.1111/rmir.12215.
- [11] D. Sanderson, D. Cox, M. Amini, A. Barbosa, Coupled urban change and natural hazard consequence model for community resilience planning, Earth's Future 10 (12) (2022), https://doi.org/10.1029/2022EF003059.
- [12] C. Zuzak, M. Mowrer, E. Goodenough, J. Burns, N. Ranalli, J. Rozelle, The National Risk Index: Establishing a Nationwide Baseline for Natural Hazard Risk in the US. Natural Hazards, 2022, https://doi.org/10.1007/s11069-022-05474-w.
- [13] G. Cremen, C. Galasso, J. McCloskey, A. Barcena, M. Creed, M.E. Filippi, R. Gentile, L.T. Jenkins, M. Kalaycioglu, E.Y. Mentese, M. Muthusamy, K. Tarbali, R.Š. Trogrlić, A state-of-the-art decision-support environment for risk-sensitive and pro-poor urban planning and design in Tomorrow's cities, Int. J. Disaster Risk Reduc. 85 (2023) 103400, https://doi.org/10.1016/j.ijdrr.2022.103400.
- [14] M. Alam, A. Barbosa, M. Scott, D. Cox, J. van de Lindt, Development of physics-based tsunami fragility functions considering structural member failures, ASCE Journal of Structure Engineering 144 (3) (2017), https://doi.org/10.1061/(ASCE)ST.1943-541X.0001953.
- [15] M. Abdelhafez, B. Ellingwood, H. Mahmoud, Vulnerability of seaports to hurricanes and Sea level rise in a changing climate: a case study for mobile, AL. Coastal Engineering (2020), https://doi.org/10.1016/j.coastaleng.2021.103884.
- [16] O. Nofal, J. van de Lindt, T. Do, G. Yan, S. Hamideh, D. Cox, C. Dietrich, Methodology for regional multihazard hurricane damage and risk assessment, ASCE Journal of Structural Engineering 147 (11) (2021), https://doi.org/10.1061/(ASCE)ST.1943-541X.0003144.
- [17] E. Fereshtehnejad, I. Gidaris, N. Rosenheim, T. Tomiczek, J. Padgett, D. Cox, S. Van Zandt, W. Peacock, Probabilistic risk assessment of coupled natural-physical-social systems: cascading impact of hurricane-induced damages to civil infrastructure in galveston, Texas, ASCE Natural Hazards Review 22 (3) (2021), https://doi.org/10.1061/(ASCE)NH.1527-6996.0000459.
- [18] P. Schneider, B. Schauer, Hazus its development and its future, ASCE Natural Hazards Review 7 (2) (2006) 40–44 https://doi.org/10.1061/(ASCE)1527-6988(2006)7:2(40.
- [19] T. McLaren, J. Myers, J. Lee, N. Tolbert, S. Hampton, C. Navarro, MAEviz an earthquake risk assessment system, Proceedings of the 16th ACE SIGSPATIAL International Conference on Advances in Geographic Information Science (2008), https://doi.org/10.1145/1463434.1463534.
- [20] J. Bai, M. Hueste, P. Gardoni, Probabilistic assessment of structural damage due to earthquakes for buildings in mid-America, 2009. ASCE Journal of Structural Engineering. 135 (10) (2009) 1155–1163 https://doi.org/10.1061/(ASCE)0733-9445, 135:10(1155.
- [21] M. Koliou, J. van de Lindt, T. McAllister, B. Ellingwood, M. Dillard, H. Cutler, State of the research in community resilience: progress and challenges, Sustainable and Resilient Infrastructure 5 (2018) 131–151. https://doi.org/10.1080/23789689.2017.1418547.
- [22] J. van de Lindt, B. Ellingwood, T. McAllister, P. Gardoni, D. Cox, W. Peacock, H. Cutler, M. Dillard, J. Lee, L. Peek, J. Mitrani-Reiser, Modeling Community Resilience: Update on the Center for Risk-Based Community Resilience Planning and the Computational Environment IN-CORE, 17th United States-Japan-New Zealand Workshop on the Improvement of Structural Engineering and Resilience (ATC-15-16), Queenstown, New Zealand, 2018. https://www.nist.gov/publications/modeling-community-resilience-update-center-risk-based-community-resilience-planning. (Accessed 10 May 2022).
- [23] G. Deierlein, S. Govindjee, F. McKenna, Overview of SimCenter goals and computational tools, in: G. Deierlein, Zsarnóczay (Eds.), State of the Art in Computation Simulation for Natural Hazard Engineering, second ed., 2021, pp. 1–9 https://doi.org/10.5281/zenodo.4558106, Zenodo.
- [24] F. Freddi, C. Galasso, G. Cremen, A. Dall' Asta, L. Di Sarno, A. Giaralis, F. Gutiérrez-Urzúa, C. Málaga-Chuquitaype, S. Mitoulis, C. Petrone, A. Sextos, L. Sousa, K. Tarbali, E. Tubaldi, J. Wardman, G. Woo, Innovations in earthquake risk reduction for resilience: recent advances and challenges, Int. J. Disaster Risk Reduc. 60 (2021), https://doi.org/10.1016/j.ijdrr.2021.102267.
- [25] V. Silva, D. Amo-Oduro, A. Calderon, C. Costa, J. Dabbeek, V. Despotaki, L. Martins, M. Pagani, A. Rao, M. Simionato, D. Viganò, C. Yepes-Estrada, A. Acevedo, H. Crowley, N. Horspool, K. Jaiswal, M. Journeay, M. Pittore, Development of a global seismic risk model, Earthq. Spectra 36 (1) (2020) 372–394, https://doi.org/10.1177/9755302010800053
- [26] C. Scheingraber, M.A. Käser, The impact of portfolio location uncertainty on probabilistic seismic risk analysis, Risk Anal. 39 (3) (2018) 695–712, https://doi.org/10.1111/risa.13176.
- [27] J. Dabbeek, H. Crowley, V. Silva, G. Weatherill, N. Paul, C.I. Nievas, Impact of exposure spatial resolution on seismic loss estimates in regional portfolios, Bull. Earthq. Eng. 19 (14) (2021) 5819–5841, https://doi.org/10.1007/s10518-021-01194-x.
- [28] E. Tate, C. Muñoz, J. Suchan, Uncertainty and sensitivity analysis of the HAZUS-MH flood model, Nat. Hazards Rev. 16 (3) (2015), https://doi.org/10.1061/
- [29] S. French, C. Barchers, W. Zhang, How should urban planners Be trained to handle big data? in: P. Thakuriah, N. Tilahun, M. Zellner (Eds.), Seeing Cities through Big Data, Springer Geography, 2017, pp. 209–217, https://doi.org/10.1007/978-3-319-40902-3_12.
- [30] P. Thakuriah, N. Tilahun, M. Zellner, Introduction to seeing cities through big data: research, methods and applications in urban informatics, in: P. Thakuriah, N. Tilahun, M. Zellner (Eds.), Seeing Cities through Big Data, 2017, pp. 1–9, https://doi.org/10.1007/978-3-319-40902-3_1.
- [31] K. Jaiswal, D. Wald, K. Porter, A global building inventory for earthquake loss estimation and risk management, Earthq. Spectra 26 (3) (2010) 731–748, https://doi.org/10.1193/1.3450316.
- [32] H. Crowley, S. Ozcebe, R. Spence, R. Foulser-Piggott, M. Erdik, K. Alten, Development of a European building inventory database, in: Proceedings of 15th World Conference on Earthquake Engineering, 2012.
- [33] F. Cacace, G. Zuccaro, D.D. Gregorio, F.L. Perelli, Building Inventory at National scale by evaluation of seismic vulnerability classes distribution based on Census data analysis: BINC procedure, Int. J. Disaster Risk Reduc. 28 (2018) 384–393, https://doi.org/10.1016/j.ijdrr.2018.03.016.
- [34] Department of Homeland Security (DHS), Homeland Infrastructure and Foundation-Level Data (HIFLD), 2021. https://hifld-geoplatform.opendata.arcgis.com/.
- [35] H. Yang, J. Yuan, D. Lunga, M. Laverdiere, A. Rose, B. Bhaduri, Building extraction at scale using convolutional neural network: mapping of the United States, IEEE J. Sel. Top. Appl. Earth Obs. Rem. Sens. 11 (8) (2018) 2600–2614, https://doi.org/10.1109/JSTARS.2018.2835377.
- [36] P. Liu, X. Liu, M. Liu, Q. Shi, J. Yang, X. Xu, Y. Zhang, Building footprint extraction from high-resolution images via spatial residual inception convolutional neural network, Rem. Sens. 11 (7) (2019), https://doi.org/10.3390/rs11070830.
- [37] J. Bennett, OpenStreetMap, Packt Publishing, 2010.
- [38] B. Neumann, A. Vafeidis, J. Zimmermann, R. Nicholls, Future coastal population growth and exposure to sea-level rise and coastal flooding a global assessment, PLoS One 10 (3) (2015), https://doi.org/10.1371/journal.pone.0118571.
- [39] I. Davies, R. Haugo, J. Robertson, P. Levin, The unequal vulnerability of communities of color to wildfire, PLoS One 13 (11) (2018), https://doi.org/10.1371/journal.pone.0205825.
- [40] T. Haer, T. Husby, W. Botzen, J. Aerts, The safe development paradox: an agent-based model for flood risk under climate change in the European Union, Global Environ. Change 60 (2020), https://doi.org/10.1016/j.gloenvcha.2019.102009.
- [41] O. Wing, W. Lehman, P. Bates, C. Sampson, N. Quinn, A. Smith, J. Neal, J. Porter, C. Kousky, Inequitable patterns of US flood risk in the Anthropocene, Nat. Clim. Change 12 (2022) 156–162, https://doi.org/10.1038/s41558-021-01265-6.
- [42] L. de Ruig, T. Haer, H. Moel, S. Brody, W. Botzen, J. Czajkowski, J. Aerts, How the USA can benefit from risk-based premiums combined with flood protection, Nat. Clim. Change (2022), https://doi.org/10.1038/s41558-022-01501-7.
- [43] N. Attary, J.W. van de Lindt, H. Mahmoud, S. Smith, C.M. Navarro, Y.W. Kim, J.S. Lee, Hindcasting community-level building damage for the 2011 Joplin EF5 tornado, Nat. Hazards 93 (3) (2018) 1295–1316, https://doi.org/10.1007/s11069-018-3353-5.

- [44] D. Cox, A. Barbosa, M. Alam, M. Amini, S. Kameshwar, H. Park, D. Sanderson, Seaside Testbed Data Inventory for Infrastructure, Population, and Earthquake-Tsunami Hazard, 2022 https://doi.org/10.17603/ds2-sp99-xv89, DesignSafe-CI.
- [45] J. Czajkowski, H. Kunreuther, E. Michel-Kerjan, Quantifying riverine and storm-surge flood risk by single-family residence: application to Texas, Risk Anal. 33 (12) (2013) 2092–2110, https://doi.org/10.1111/risa.12068.
- [46] M. Roohi, J. van de Lindt, N. Rosenheim, Y. Hu, H. Cutler, Implication of building inventory accuracy on physical and socio-economic resilience metrics for informed decision-making in natural hazards, Structure and Infrastructure Engineering 17 (4) (2020) 534–554, https://doi.org/10.1080/15732479.2020.1845753.
- [47] Q. Yu, C. Wang, B. Cetiner, S.X. Yu, F. Mckenna, E. Taciroglu, K.H. Law, Building Information Modeling and Classification by Visual Learning at A City Scale, 2019 https://doi.org/10.48550/ARXIV.1910.06391, arXiv.
- [48] P.A. Pelizari, C. Geiß, P. Aguirre, H.S. María, Y.M. Peña, H. Taubenböck, Automated building characterization for seismic risk assessment using street-level imagery and deep learning, ISPRS J. Photogrammetry Remote Sens. 180 (2021) 370–386, https://doi.org/10.1016/j.isprsjprs.2021.07.004.
- [49] C. Barbaros, C. Wang, F. McKenna, S. Hornauer, Y. Guo, [Software]. BRAILS Release v3.0.0. https://doi.org/10.5281/zenodo.7132010, 2022.
- [50] A. Enderami, R. Mazumder, M. Dumler, E. Sutley, Virtual testbeds for community resilience analysis: state-of-the-art review, consensus study, and recommendations, ASCE Natural Hazards Review 23 (4) (2022), https://doi.org/10.1061/(ASCE)NH.1527-6996.0000582.
- [51] A. Zsarnóczay, G.G. Deierlein, C.J. Williams, T.L. Kijewski-Correa, A.-M. Esnard, L.N. Lowes, L. Johnson, Community perspectives on simulation and data needs for the study of natural hazard impacts and recovery, Nat. Hazards Rev. 24 (1) (2023), https://doi.org/10.1061/nhrefo.nheng-1551.
- [52] S. Shultz, Accuracy of HAZUS general building stock data, Nat. Hazards Rev. 18 (4) (2017), https://doi.org/10.1061/(asce)nh.1527-6996.0000258.
- [53] R.B. Mostafiz, C.J. Friedland, M.A. Rahman, R.V. Rohli, E. Tate, N. Bushra, A. Taghinezhad, Comparison of neighborhood-scale, residential property flood-loss assessment methodologies, Front. Environ. Sci. 9 (2021), https://doi.org/10.3389/fenvs.2021.734294.
- [54] E. Yildirim, C. Just, I. Demir, Flood risk assessment and quantification at the community and property level in the State of Iowa, Int. J. Disaster Risk Reduc. 77 (2022) 103106, https://doi.org/10.1016/j.ijdrr.2022.103106.
- [55] T. Kijewski-Correa, B. Cetiner, K. Zhong, C. Wang, A. Zsarnoczay, Y. Guo, M. Lochhead, F. McKenna, Validation of an augmented parcel approach for hurricane regional loss assessments, Nat. Hazards Rev. 24 (3) (2023), https://doi.org/10.1061/nhrefo.nheng-1649.
- [56] U.S. Census Bureau, Table DP05: ACS Demographic and Housing Estimates, 2022 Retrieved from. https://data.census.gov/cedsci/.
- [57] C. Goldfinger, H. Nelson, A. Morey, J. Johnson, J. Patton, E. Karabanov, J. Gutiérrez-Pastor, A. Eriksson, E. Gràcia, G. Dunhill, R. Enkin, A. Dallimore, T. Vallier, Turbidite Event History Methods and Implications for Holocene Paleoseismicity of the Cascadia Subduction Zone, US Geological Survey Professional, 2012 Paper 1661-F. 170pp. https://pubs.er.usgs.gov/publication/pp1661F.
- [58] Oregon Seismic Safety Policy Advisory Commission (OSSPAC), "The Oregon resilience plan: reducing risk and improving recovery for the next Cascadia subduction earthquake and tsunami". Salem, Oregon, https://www.oregon.gov/oem/documents/oregon_resilience_plan_final.pdf, 2013. (Accessed 16 June 2022).
- [59] H. Park, D. Cox, M. Alam, A. Barbosa, Probabilistic seismic and tsunami hazard analysis conditioned on a megathrust rupture of the Cascadia subduction zone, Frontiers in Built Environment 3 (32) (2017), https://doi.org/10.3389/fbuil.2017.00032.
- [60] H. Park, D. Cox, A. Barbosa, Comparison of inundation depth and momentum flux based fragilities for probabilistic tsunami damage assessment and uncertainty analysis, Coast Eng. 122 (2017) 10–26, https://doi.org/10.1016/j.coastaleng.2017.01.008.
- [61] H. Park, M. Alam, D. Cox, A. Barbosa, J. van de Lindt, Probabilistic seismic and tsunami damage analysis (PSTDA) of the Cascadia Subduction Zone applied to Seaside, Oregon, Int. J. Disaster Risk Reduc. 35 (2019), https://doi.org/10.1016/j.ijdrr.2019.101076.
- [62] S. Kameshwar, D. Cox, A. Barbosa, K. Farokhnia, H. Park, M. Alam, J. van de Lindt, Probabilistic decision-support framework for community resilience: incorporating multi-hazards, infrastructure interdependencies, and resilience goals in a Bayesian network, Reliab. Eng. Syst. Saf. 191 (2019), https://doi.org/ 10.1016/j.ress.2019.106568.
- [63] N. Rosenheim, R. Guidotti, P. Gardoni, W. Peacock, Integration of detailed household and housing unit characteristic data with critical infrastructure for post-hazard resilience modeling, Sustainable and Resilient Infrastructure (6) (2019), https://doi.org/10.1080/23789689.2019.1681821.
- [64] D. Sanderson, D. Cox, G. Naraharisetty, A Spatially Explicit Decision Support Framework for Parcel- and Community-Level Risk and Resilience Assessment Using Bayesian Networks. Sustainable And Resilient Infrastructure, 2021, https://doi.org/10.1080/23789689.2021.1966164.
- [65] D. Sanderson, S. Kameshwar, N. Rosenheim, D. Cox, Deaggregation of multi- hazard damages, losses, risks, and connectivity: an application to the joint seismic-tsunami hazard at Seaside, Oregon, Nat. Hazards 109 (2) (2021) 1821–1847, https://doi.org/10.1007/s11069-021-04900-9.
- [66] A. Beck, H. Talebiyan, E. Cha, L. Dueñas-Osorio, Comparative Retrofit Prioritization Schemes for Electric Power Networks: Application to the Community in Seaside, OR. 8th International Symposium On Reliability Engineering And Risk Management, 2022, https://doi.org/10.3850/978-981-18-5184-1_MS-18-096-cd.
- [67] M. Amini, D. Sanderson, D. Cox, A. Barbosa, Methodology to incorporate seismic damage and debris to evaluate strategies to reduce life safety risk for multi-hazard earthquake and tsunami, Manuscript submitted to Natural Hazards [preprint] (2023), https://doi.org/10.1007/s11069-023-05937-8.
- [68] U.S. Bureau of Labor Statistics, Consumer Price Index Inflation Calculator, U.S. Department of Labor, 2023. https://www.bls.gov/data/inflation_calculator.htm
- [69] Bing Maps Team, Computer Generated Building Footprints for the United States. Github, 2018. https://github.com/microsoft/USBuildingFootprints.
- [70] Federal Emergency Management Agency (FEMA), Hazus Inventory Technical Manual, Hazus 4.2 Service Pack 3, Washington, D.C, 2021.
- [71] Federal Emergency Management Agency (FEMA), Hazus Inventory Technical Manual. Hazus, 6.0, 2022 Washington, D.C.
- [72] R. Gentile, G. Cremen, C. Galasso, L. Jenkins, V. Manandhar, E. Mentese, R. Guragain, J. McCloskey, Scoring, selecting, and developing physical impact models for multi-hazard risk assessment, Int. J. Disaster Risk Reduc. 82 (2022), https://doi.org/10.1016/j.ijdrr.2022.103365.
- [73] W. Wang, J. van de Lindt, H. Cutler, N. Rosenheim, M. Koliou, J. Lee, D. Calderon, Community resilience assessment of an EF-5 tornado using the IN-CORE modeling environment, in: Life-Cycle Civil Engineering: Innovation, Theory and Practice, CRC Press, 2021, pp. 394–398, https://doi.org/10.1201/9780429343292
- [74] M. Shinozuka, M. Feng, J. Lee, T. Naganuma, Statistical analysis of fragility curves, ASCE Journal of Engineering Mechanics 126 (12) (2000) 1224–1231 https://doi.org/10.1061/(ASCE)0733-9399, 2000)126:12(1224.
- [75] Federal Emergency Management Agency (FEMA), Hazus Earthquake Model Technical Manual, Hazus 4.2 Service Pack 3, Washington, D.C., 2020.
- [76] Federal Emergency Management Agency (FEMA), Hazus Tsunami Model Technical Manual, Hazus 4.2 Service Pack 3, Washington, D.C, 2021.
- [77] M. Modarres, M. Kaminskiy, V. Krivtsov, Reliability Engineering and Risk Analysis: a Practical Guide, CRC Press, Boca Raton, Florida, 2016.
- [78] U.S. Census Bureau, Glossary. United States Census Bureau, 2022. https://www.census.gov/glossary/.
- [79] A. Saltelli, M. Ratto, T. Andres, F. Campolongo, J. Cariboni, D. Gatelli, M. Saisana, S. Tarantola, Global Sensitivity Analysis: the Primer, John Wiley and Sons Ltd. 2008.
- [80] U.S., Army Corps of Engineers, National Structure Inventory, 2023. https://www.hec.usace.army.mil/confluence/nsi/.
- [81] W. Wang, J. van de Lindt, Quantitative modeling of residential building disaster recovery and effects of pre- and post-event policies, Int. J. Disaster Risk Reduc. 59 (2021), https://doi.org/10.1016/j.ijdrr.2021.102259.
- [82] W. Wang, J. van de Lindt, Quantifying the effect of improved school and residential building codes for tornadoes in community resilience, Resilient Cities and Structures 1 (1) (2022) 65–79, https://doi.org/10.1016/j.rcns.2022.04.001.